In vivo photoacoustic imaging of prostate brachytherapy seeds

Muyinatu A. Lediju Bell*[a], Nathanael P. Kuo[b], Danny Y. Song[c], Jin Kang[d], and Emad M. Boctor[a,e]

[a]Johns Hopkins University, Department of Computer Science, Baltimore, MD, USA;
[b]Johns Hopkins University, Department of Biomedical Engineering, Baltimore, MD, USA;
[c]Johns Hopkins University School of Medicine, Department of Radiation Oncology, Baltimore, MD, USA;
[d]Johns Hopkins University, Department of Electrical Engineering and Computer Science, Baltimore, MD, USA;
[e]Johns Hopkins University, School of Medicine, Department of Radiology, Baltimore, MD, USA

ABSTRACT

We conducted an approved canine study to investigate the *in vivo* feasibility of photoacoustic imaging for intraoperative updates to brachytherapy treatment plans. Brachytherapy seeds coated with black ink were inserted into the canine prostate using methods similar to a human procedure. A transperineal, interstitial, fiber optic light delivery method, coupled to a 1064 nm laser, was utilized to irradiate the prostate and the resulting acoustic waves were detected with a transrectal ultrasound probe. The fiber was inserted into a high dose rate (HDR) brachytherapy needle that acted as a light-diffusing sheath, enabling radial light delivery from the tip of the fiber inside the sheath. The axis of the fiber was located at a distance of 4-9 mm from the long axis of the cylindrical seeds. Ultrasound images acquired with the transrectal probe and post-operative CT images of the implanted seeds were analyzed to confirm seed locations. *In vivo* limitations with insufficient light delivery within the ANSI laser safety limit (100 mJ/cm^2) were overcome by utilizing a short-lag spatial coherence (SLSC) beamformer, which provided average seed contrasts of 20-30 dB for energy densities ranging 8-84 mJ/cm^2. The average contrast was improved by up to 20 dB with SLSC beamforming compared to conventional delay-and-sum beamforming. There was excellent agreement between photoacoustic, ultrasound, and CT images. Challenges included visualization of photoacoustic artifacts that corresponded with locations of the optical fiber and hyperechoic tissue structures.

Keywords: brachytherapy, dynamic dosimetry, intraoperative treatment planning, photoacoustic, optoacoustic, image-guided intervention

1. INTRODUCTION

Brachytherapy is a popular treatment option for prostate cancer, administered by permanently implanting approximately 80-120 tiny seeds according to a predefined treatment plan.[1,2] The seeds are filled with a radioactive substance, and each treatment plan is designed to maximize dose to cancerous regions while sparing healthy tissue.[3,4] Although brachytherapy has excellent five- to ten-year treatment outcomes,[5–7] complications typically arise when there is a mismatch between the planned and delivered doses caused by factors such as seed migration, prostate motion, edema, or surgeon-dependent implantation errors.[8,9] The potential for a mismatch between planned and delivered doses can be avoided with a treatment planning approach that allows dynamic, intraoperative updates to the original treatment plan.[6,10]

The first step toward intraoperative treatment planning is real-time seed localization, which is currently performed with transrectal ultrasound imaging.[11,12] Yet, seeds are often difficult to locate with ultrasound due to factors such as the small size of the seeds and the presence of calcifications that may be mistaken for seeds. In addition, inherent acoustic artifacts such as shadowing from the required placement of a urinary catheter or sound

*E-mail: muyinatu.ledijubell@jhu.edu

Photons Plus Ultrasound: Imaging and Sensing 2014, edited by Alexander A. Oraevsky, Lihong V. Wang,
Proc. of SPIE Vol. 8943, 894348 · © 2014 SPIE · CCC code: 1605-7422/14/$18 · doi: 10.1117/12.2040817

reverberations in the presence of many seeds present challenges for seed localization.[13,14] Thus, post operative computed tomography (CT) images are conventionally employed to confirm seed locations and determine if alternative forms of treatment (e.g. external beam therapy) are needed to compensate for underdosed regions of the prostate.[15] This approach increases the risks associated with radiation exposure and does not address complications that may occur with overdosing healthy tissue, such as urinary incontinence, rectal damage, or erectile dysfunction.[4] It is less likely that over- or under-dosage will occur if seeds are better visualized during an operation.

Photoacoustic imaging has potential to complement ultrasound detection of brachytherapy seeds and overcome current limitations with intraoperative seed visualization.[16–18] It is based on light transmission and optical absorption of a target, which subsequently undergoes thermoelastic expansion and generates associated sound waves that are detectable with conventional ultrasound transducers.[19] Thus, the main additional hardware required to introduce photoacoustic imaging into a clinical brachytherapy suite is a laser system that transmits nanosecond light pulses. The light is absorbed by the seeds and the resulting sound waves may be detected with the same transrectal ultrasound probe that is used for seed and needle visualization. Excellent seed contrast is expected with photoacoustic imaging because the optical absorption of the seeds is significantly larger than that of surrounding tissue.[17]

Several researchers previously assessed the feasibility of seed visualization with photoacoustic imaging, noting properties such as sensitivity to seed orientation,[17,20] sufficient light penetration in prostatic tissue,[17] isolation of seed-related signals from blood-related signals at a laser wavelength of 1064 nm,[16] and enhanced seed contrast with a highly optically absorbing coating.[21] Our previous work additionally demonstrated the concepts of transperineal light delivery and short-lag spatial coherence (SLSC) beamforming to increase seed contrast in the presence of minimal laser fluence.[22] Conclusions drawn from these feasibility studies were based on phantom and *ex vivo* data.

This paper builds on previous work by translating a customized photoacoustic system to an animal operating room and testing the transperineal light delivery method on an *in vivo* canine prostate in the presence of blood, proteins, and other endogenous chromophores. To the authors' knowledge, this work is the first to demonstrate the *in vivo* feasibility of visualizing prostate brachytherapy seeds with combined photoacoustic and ultrasound imaging.

2. METHODS AND MATERIALS

2.1 Imaging Equipment

The ultrasound equipment consisted of three main components manufactured by Ultrasonix (Richmond, BC, Canada). A SonixTouch ultrasound scanner was connected to a SonixDAQ data acquisition unit to access raw pre-beamformed radiofrequency (RF) data. The sample acquisition rate of the SonixDAQ was 40 MHz. The ultrasound scanner was additionally connected to a transrectal ultrasound probe with linear (BPL9-5/55) and curvilinear (BPC8-4/10) arrays containing 128 elements each with center frequencies of 7 MHz and 6 MHz, respectively.

To acquire photacoustic images, the SonixDAQ was triggered by the flashlamp output signal of a Phocus neodymium-doped yttrium aluminum garnet (Nd:YAG) laser manufactured by Quantel (Bozeman, MT, USA) with an optical parametric oscillator installed by Opotek (Carlsbad, CA). The laser repetition rate was 10 Hz with a 5 ns pulse duration.

The laser beam was air-coupled into a 1 mm core diameter optical fiber with a numerical aperture of 0.37 (Newport F-MBE, Irvine, CA). The laser and all optical components were secured on a portable optical table (Thorlabs, NJ, USA) for mobility in the operating room. The optical table was enclosed in a black box with a small hole to expose the optical fiber. The exposed fiber was inserted into a hollow, plastic, high-dose-rate (HDR) brachytherapy needle of inner diameter 1.5 mm and outer diameter 2.0 mm (ProGuide 6F sharp, manufactured by Nucletron, Veenendaal, The Netherlands). This HDR brachytherapy needle acted as a light-diffusing sheath that enabled light delivery within a 2 cm radius of the fiber tip, as confirmed by coupling visible laser light (635 nm) to the fiber and observing the beam pattern in air before and after the free end of the fiber was inserted into the sheath.

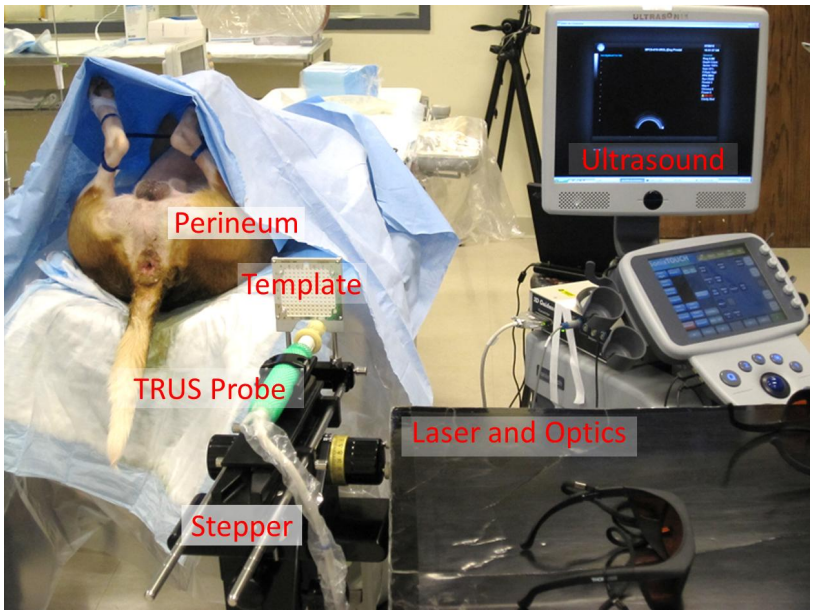

(a)

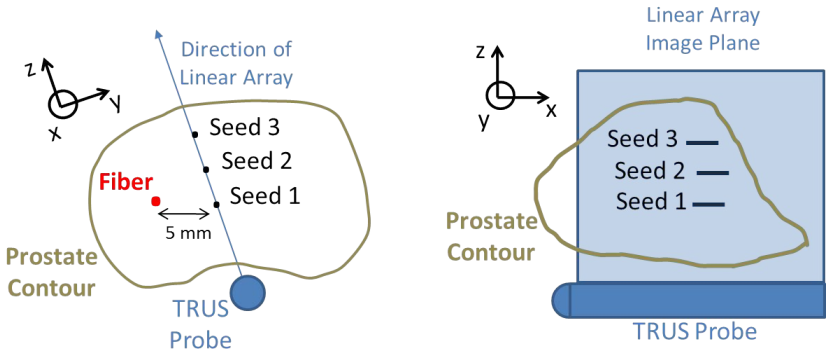

(b)

Figure 1. (a) Experimental equipment for *in vivo* imaging of a canine prostate. (b) Orientation of three implanted coated seeds relative to optical fiber and TRUS probe (not drawn to scale).

The ultrasound and photoacoustic systems were used to acquire beamformed RF pulse-echo ultrasound data and pre-beamformed photoacoustic data, respectively. Ultrasound and photoacoustic data were collected with the linear (BPL9-5/55) and curvilinear (BPC8-4/10) arrays of the TRUS probe. The transmit frequency for pulse-echo ultrasound was 6.6 MHz with the linear array and 6.0 MHz with the curvilinear array. The primary wavelength of the Nd:YAG laser, 1064 nm, was used to distinguish photoacoustic signals from blood.[16] Five frames of photoacoustic data were recorded for each acquisition.

A Philips (Andover, MA) XperCT scanner was utilized to acquire post operative CT images of the canine prostate. Each image in the volume stack was 384 pixels x 384 pixels with a 0.5 mm spacing between pixels.

2.2 *In Vivo* Experiment

A 25 kg dog was prepared for a prostate brachytherapy procedure approved by the Johns Hopkins Animal Care and Use Committee (Protocol #DO13M143). After sedation and intravenous induction, anesthesia was maintained with continuous inhalation of 1-3% isoflurane. The perineum was shaved and a urinary catheter was inserted. The dog was positioned supine with its legs immobilized and a cover was draped over the dog, as shown in Fig. 1(a). The dog was continuously monitored throughout the procedure.

A portable Nucletron prostate stepper (Veenendaal, The Netherlands) was used to hold the transrectal ultrasound probe. A Nucletron prostate stepper template for HDR brachytherapy with a square grid of holes separated by 5 mm was attached to the stepper, as shown in Fig. 1(a). The grid was then aligned with the perineum and the stepper was locked in place. After protecting the transrectal ultrasound probe with a sanitized latex probe cover, it was inserted in the rectum to visualize the prostate.

A standard 18G brachytherapy needle (Bard, Brachystar, Covington, GA), consisting of a hollow outer cannula and removable inner stylet, was inserted through one of the holes in the template, through the perineum, and into the prostate under transrectal ultrasound guidance. Non-radioactive, titanium, cylindrical brachytherapy seeds of length of 4.5 mm and outer diameter 0.8 mm (TheraSeed, Theragenics Corporation, Buford, GA, USA) were previously painted with black India Ink to increase optical absorption. Three seeds were deposited into the prostate using standard brachytherapy seed insertion procedures.

The light diffusing sheath described previously was inserted through the template grid and perineum with the aid of a stiff guide needle that is typically used in HDR brachytherapy procedures. The guide needle was then removed and replaced with the 1 mm optical fiber. The light diffusing sheath containing the optical fiber was positioned parallel to the seeds at a distance of approximately 5 mm from Seed #1, as shown in Fig. 1(b).

Photoacoustic imaging was performed with the energy at the tip of the sheathed fiber varied from 0.5-10.5 mJ per pulse. The corresponding energy densities are reported in Table 1. Energy densities were calculated using a conical sheath tip approximation with a cone slant height of 2 mm and base diameter of 2 mm. Co-registered pulse-echo RF ultrasound data were acquired with each photoacoustic image. CT images were acquired after the operation to confirm seed locations.

Table 1. Relationship between energy measured at the tip of the fiber surrounded by the light-diffusing sheath and corresponding energy densities, using a conical sheath tip approximation.

Energy per pulse (mJ)	0.5	1.1	2.0	2.5	3.5	4.3	5.3	6.0	6.8	7.7	9.0	9.9	10.5
Energy Density (mJ/cm^2)	8	18	32	40	56	68	84	95	108	123	143	158	167

2.3 Image Formation

A conventional delay-and-sum (DAS) beamformer and a coherence-based SLSC beamformer[22,23] were applied to the received photoacoustic signals. Received signal time delays were calculated with 33-element subapertures for the DAS and SLSC photoacoustic images. The short-lag integral was 12% of the number of elements in the receive aperture (i,e, 4 elements). Hanning apodization was applied to the delayed signals for DAS beamforming. No apodization was applied for SLSC beamforming. Beamformed ultrasound and PA data were envelope-detected, normalized to the brightest image pixel, and log compressed. In addition, images acquired with the curvilinear array were scan converted. Paired DAS and SLSC images were displayed with the same dynamic range. No frame averaging was applied to display the images. All image processing was performed with MATLAB software (The MathWorks, Inc., Natick, MA).

2.4 Image Analysis

Seed contrast and signal-to-noise ratios (SNR) in ultrasound and photoacoustic images were calculated using the following equations:

$$\text{Contrast} = 20\log_{10}\left(\frac{S_i}{S_o}\right) \quad (1)$$

$$\text{SNR} = \frac{S_i}{\sigma_o} \quad (2)$$

where S_i and S_o are the means of the image data within regions of interest (ROIs) located inside and outside of the brachytherapy seed, respectively, and σ_o is the standard deviation of the data within the ROI located outside of the seed. Rectangular ROIs surrounding the maximum signal from the seed were manually selected for each seed in each image evaluated, and a matching ROI at the same depth and with the same size was automatically created, starting at a fixed lateral position to the right of the seed. The fixed lateral position was the same

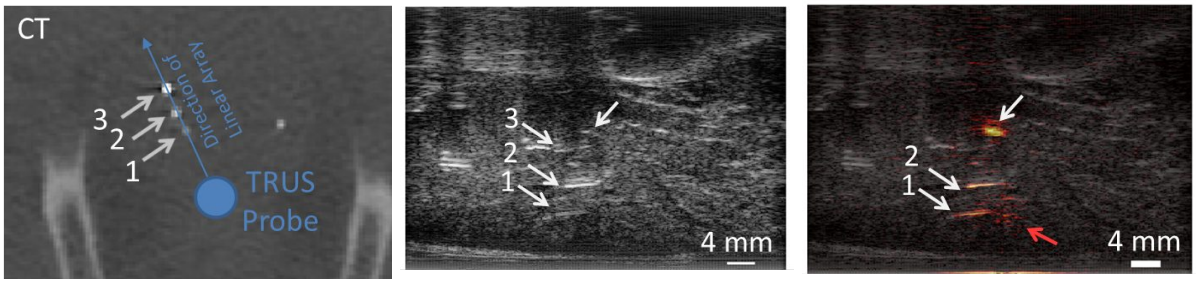

(a) (b) (c)

Figure 2. Visualization of multiple coated brachytherapy seeds with (a) post operative CT, (b) conventional ultrasound imaging, and (c) corresponding photoacoustic images overlaid on ultrasound images in a yellow-red color scale. The energy density at the fiber tip for the photoacoustic images was 123 mJ/cm^2, respectively. Unlabeled arrows point to the photoacoustic response from the location of the fiber (red arrow) and a signal of unknown origin (white arrow).

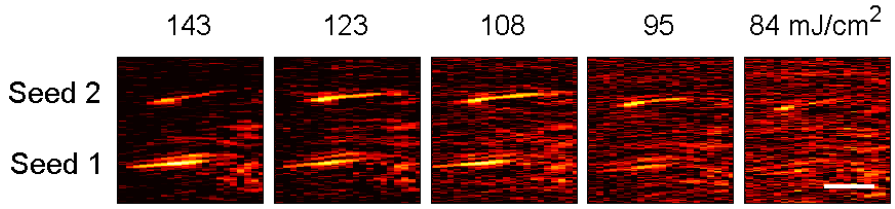

(a)

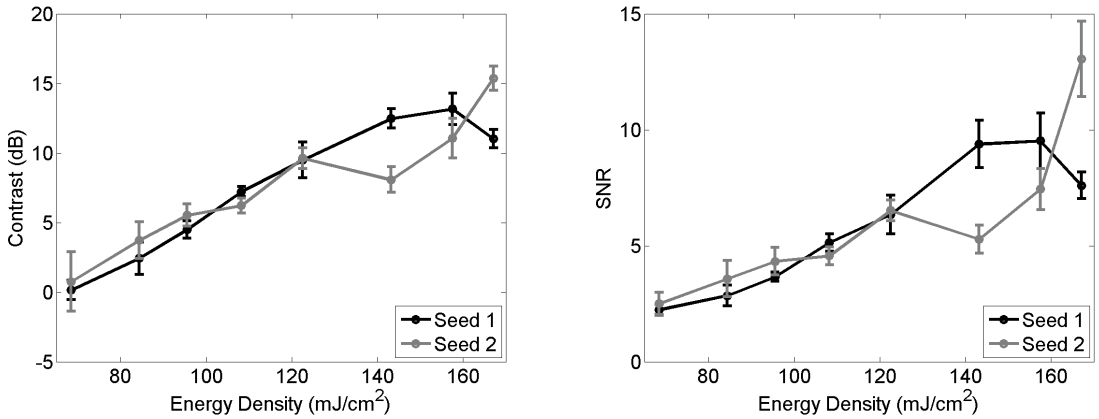

(b) (c)

Figure 3. (a) Photoacoustic images of the seeds in Fig. 2 as a function of energy density at the sheath tip surrounding the optical fiber. All images are shown with 20 dB dynamic range. The scale bar shows 4 mm. (b) Contrast and SNR as a function of energy density at the sheath tip surrounding the optical fiber. Results were averaged over five trials. Error bars show ± one standard deviation.

in paired SLSC and DAS beamformed PA images. The average ROI size ± one standard deviation was 1.4 ± 0.5 mm (axial) x 3.2 ± 1.0 mm (lateral) in SLSC and DAS photoacoustic images. The average lateral distance between the right edge of the seed ROI and the left edge of the noise ROI (i.e. the ROI located outside of the seed) was 6 mm.

The 3D locations of the implanted seeds were identified in the postoperative CT images. The relative distance between seeds was measured in photoacoustic and ultrasound images for comparison with CT images. Ultrasound and photoacoustic image analyses were performed with MATLAB software (The MathWorks, Inc., Natick, MA) while CT image analyses were performed with ImageJ software.

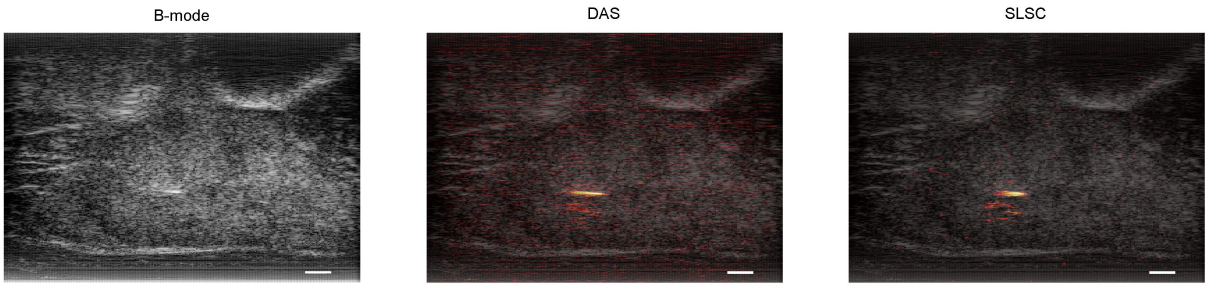

(a) (b) (c)

Figure 4. Visualization of one coated brachytherapy seed at an average sheath tip energy density of 48 mJ/cm^2. DAS and SLSC images are overlaid on B-mode images and shown with 15dB dynamic range. A photoacoustic response from the location of the fiber appears below the seed.The scale bar shows 4 mm.

3. RESULTS

The diameters of three implanted brachytherapy seeds were visible in axial slices of the post operative CT image, as demonstrated in Fig. 2 (a). The location of the transrectal ultrasound probe at the time of the experiment is represented by the blue circle. The seeds were numbered with seed #1 located closest to the probe. The linear array of the TRUS probe was rotated to the direction shown in Fig. 2 (a) to visualize the three seeds in ultrasound and photoacoustic images.

The long axes of the seeds were visualized with the linear array of the TRUS probe, as shown in Fig. 2 (b) with arrows indicating seeds # 1, 2, and 3. Although it is difficult to visualize these seeds due to their small size and limited acoustic contrast with the prostatic tissue, their locations were more obvious during the operation, as they were inserted.

A co-registered photoacoustic image is overlaid on the ultrasound image in a yellow-red color scale in Fig. 2 (c). Two of the three seeds are better visualized in the photoacoustic image (seeds # 1 and 2), in addition to a signal that appears to correlate with tissue structure in the ultrasound image (unlabeled white arrows). There is additionally a fainter signal that corresponds with the location of the out-of-plane fiber (red arrow). The axial spacing between seeds #1 and 2 is 3.82 mm in the photoacoustic and ultrasound images, which corresponds with the 4 mm seed spacing measured along the direction of the linear array shown in the post operative CT image.

The two visible seeds in the photoacoustic image of Fig. 2 (c) are shown in Fig. 3(a) as the energy at the fiber tip was varied from 68-167 mJ/cm^2. Contrast and SNR were measured as a function of energy density at the fiber tip for these two seeds. As shown in Figs. 3(b) and 3(c), contrast and SNR are generally higher at higher energy densities. Results indicate that the seeds are difficult to visualize when the contrast and SNR are below 5 dB and 4, respectively, which occurs for energy densities less than or equal to 95 mJ/cm^2. Note that the ANSI laser safety limit for a 1064 nm laser wavelength is 100 mJ/cm^2, and the seeds are barely visible within this limit.

One approach to overcome the poor contrast at lower laser energies is to implement SLSC beamforming. An independent data set was acquired to test this approach. One coated brachytherapy seed was implanted approximately 4 mm from the fiber, as confirmed in images acquired with the curvilinear array. The fiber was not visible in the ultrasound B-mode image when the linear array was facing the seed, as shown in Fig. 4(a). Similar to previous results, it is difficult to visualize the seed in this ultrasound image due to its small size and poor acoustic contrast. The seed is better visualized in the corresponding photoacoustic images (Fig. 4(b) and 4(c)), along with an artifact from the out-of-plane fiber located below the seed. Note that the SLSC beamformed image has less background noise than the DAS image when both PA images are shown with the same dynamic range. The laser energy for these images measured 3.5 mJ, which corresponds to an energy density of 48 mJ/cm^2.

The laser energy was varied from 8-167 mJ/cm^2 and corresponding photoacoustic images of the single seed are shown in Fig. 5 (a). Seed contrast and SNR were measured in these images as a function of energy, as reported in Fig. 5(b) and (c), respectively. Results demonstrate that the SLSC beamformer has up to 20 dB

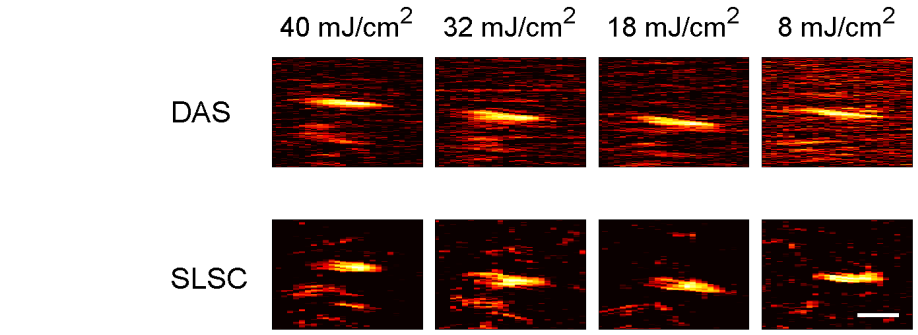

(a)

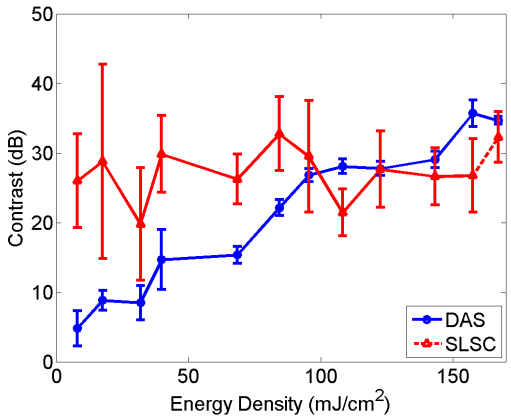

(b)

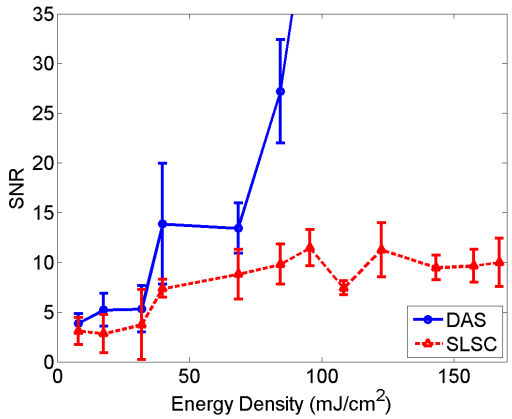

(c)

Figure 5. (a) Contrast and (b) SNR measurements as a function of energy density at the sheath tip for the seed shown in Fig. 4. The SLSC beamformer produces images with greater contrast and similar SNR at the lower energy densities. Measurements were averaged over 3-5 trials. Error bars show ± one standard deviation.

better contrast and similar SNR to DAS beamformed images when the laser energies are below the ANSI safety limit of 100 mJ/cm^2. At energies beyond this safety limit, the SNR of DAS images is approximately 3-12 times better than that of SLSC images. A majority of these SNR values for the DAS beamformer exceed the scale shown in Fig. 5 (c).

4. DISCUSSION

The *in vivo* feasibility of visualizing prostate brachytherapy seeds for intraoperative treatment planning with combined ultrasound and photoacoustic imaging was assessed with an interstitial light delivery method and a transrectal ultrasound probe. Seeds were visualized within the ANSI laser safety limit for human exposure (100 mJ/cm^2 for 1064 nm laser wavelength[26]) when the axis of the fiber was located at a distance of approximately 4 mm from the long axis of the cylindrical seeds (Figs. 4 and 5). These results suggest that any seed within at least 4 mm of the long axis of the fiber has potential to be visualized in human patients.

Low-contrast images were enhanced with the SLSC beamformer compared to images created with a more conventional amplitude-based DAS beamformer. The SLSC beamformer calculates the spatial coherence of the received acoustic wavefield, and is therefore less susceptible to insufficient laser fluence. *In vivo* application of this beamformer provided average seed contrasts of 20-30 dB, which agrees with our previous observations in phantoms and *ex vivo* tissue.[22] The energy densities over which this contrast was achieved ranged 8-84 mJ/cm^2, which is 8-84% of the ANSI safety limit.

The visualization of photoacoustic signals that do not correspond with seed locations presents a challenge for *in vivo* imaging and clinical translation to humans. One example is the persistence of an artifact due to the scattering of light concentrated near the fiber tip, despite the fiber being in a different imaging plane. Visualization of these fiber-related signals can be regarded as an opportunity for intraoperative localization of the fiber tip. Advanced filters may then be applied to suppress this signal after the location of the fiber tip has been identified. In addition, as shown in Fig. 5 with 8 mJ/cm^2 energy density, the SLSC beamformer may be implemented to suppress the signal caused by the fiber if the magnitude of the fiber-related signal is similar to that of the background noise.

Additional photoacoustic signals appear to correlate with identifiable tissue structures in co-registered ultrasound images. We hypothesize that these signals are artifacts caused by acoustic interactions with the multiple echogenic structures within the prostate that coincidentally correlate with tissue structures and constructively interfere to make a bright appearance. These photoacoustic signals are likely to appear as false positives for intraoperative detection of brachytherapy seeds. Shape-based filters may be applied based on expected seed orientations and related expectations of the photoacoustic response to minimize these false positives.

One embodiment of the proposed technique translated to human patients could be insertion of multiple plastic HDR brachytherapy needles (i.e. light diffusing sheaths) in different regions of the prostate for the duration of a brachytherapy procedure. An optical fiber may then be inserted into any one of the sheaths and translated inside the sheath along the longitudinal direction of the prostate, as previously demonstrated with phantom experiments.[22] This method allows for selective regional visualization of implanted seeds.

5. CONCLUSION

For the first time, we demonstrated the *in vivo* feasibility of visualizing coated prostate brachytherapy seeds with photoacoustic imaging, utilizing a transperineal interstitial laser delivery method and a transrectal ultrasound probe. Co-registered ultrasound and photoacoustic images were acquired to confirm seed locations. Additional confirmation was provided with a post operative CT image of the implanted seeds. An advanced SLSC beamformer was used to visualize seeds subject to insufficient local laser fluence and suppress fiber-related signals at lower laser energies. Results are encouraging for eventual translation to humans.

ACKNOWLEDGMENTS

M. A. Lediju Bell is a recipient of the Ford Foundation and UNCF/Merck Postdoctoral fellowships. Additional funding was provided by discretionary funds from the Johns Hopkins Department of Radiology and NIH grants CA180561 and EB015638. Special thanks to Dawn Ruben, Laurie Pipitone, Behnoosh Tavakoli, Xiaoyu Guo, and Anastasia Ostrowski.

REFERENCES

[1] PJ Hoskin. Prostate cancer: permanent low dose rate seed brachytherapy and temporary high dose rate afterloading brachytherapy. *Radiotherapy in Practice-Brachytherapy*, page 103, 2011.

[2] J Crook. The role of brachytherapy in the definitive management of prostate cancer. *Cancer/Radiothérapie*, 15(3):230–237, 2011.

[3] John C Blasko, Peter D Grimm, John E Sylvester, Kas Ray Badiozamani, David Hoak, and William Cavanagh. Palladium-103 brachytherapy for prostate carcinoma. *International Journal of Radiation Oncology* Biology* Physics*, 46(4):839–850, 2000.

[4] John C Blasko, Peter D Grimm, John E Sylsvester, and William Cavanagh. The role of external beam radiotherapy with i-125/pd-103 brachytherapy for prostate carcinoma. *Radiotherapy and Oncology*, 57(3):273–278, 2000.

[5] Juanita Crook, Jette Borg, Andrew Evans, Ants Toi, EP Saibishkumar, Sharon Fung, and Clement Ma. 10-year experience with i-125 prostate brachytherapy at the princess margaret hospital: results for 1,100 patients. *International Journal of Radiation Oncology* Biology* Physics*, 80(5):1323–1329, 2011.

[6] Michael J Zelefsky, Yoshiya Yamada, Gilad N Cohen, Alison Shippy, Heather Chan, David Fridman, and Marco Zaider. Five-year outcome of intraoperative conformal permanent i-125 interstitial implantation for patients with clinically localized prostate cancer. *International Journal of Radiation Oncology* Biology* Physics*, 67(1):65–70, 2007.

[7] Michael Buckstein, Todd J Carpenter, Nelson N Stone, and Richard G Stock. Long-term outcomes and toxicity in patients treated with brachytherapy for prostate adenocarcinoma younger than 60 years of age at treatment with minimum 10 years of follow-up. *Urology*, 81(2):364–369, 2013.

[8] L Potters, XH Wang, and Y Yamada. A nomogram to compensate for intraoperative prostate edema during transperineal brachytherapy. *Techniques in urology*, 6(2):99, 2000.

[9] Edward M Messing, JBY Zhang, Deborah J Rubens, Ralph A Brasacchio, John G Strang, Arvind Soni, MC Schell, Paul G Okunieff, and Yan Yu. Intraoperative optimized inverse planning for prostate brachytherapy: Early experience. *International Journal of Radiation Oncology* Biology* Physics*, 44(4):801–808, 1999.

[10] Subir Nag, Jay P Ciezki, Robert Cormack, Stephen Doggett, Keith DeWyngaert, Gregory K Edmundson, Richard G Stock, Nelson N Stone, Yan Yu, and Michael J Zelefsky. Intraoperative planning and evaluation of permanent prostate brachytherapy: report of the american brachytherapy society. *International Journal of Radiation Oncology* Biology* Physics*, 51(5):1422–1430, 2001.

[11] Alfredo Polo, Carl Salembier, Jack Venselaar, and Peter Hoskin. Review of intraoperative imaging and planning techniques in permanent seed prostate brachytherapy. *Radiotherapy and Oncology*, 94(1):12–23, 2010.

[12] Arjun Sahgal and Mack Roach. Permanent prostate seed brachytherapy: a current perspective on the evolution of the technique and its application. *Nature Clinical Practice Urology*, 4(12):658–670, 2007.

[13] SEM Langley and R Laing. Prostate brachytherapy has come of age: a review of the technique and results. *BJU international*, 89(3):241–249, 2002.

[14] Ben H Han, Kent Wallner, Gregory Merrick, Wayne Butler, Steven Sutlief, and John Sylvester. Prostate brachytherapy seed identification on post-implant trus images. *Medical physics*, 30:898, 2003.

[15] Subir Nag, William Bice, Keith DeWyngaert, Bradley Prestidge, Richard Stock, and Yan Yu. The american brachytherapy society recommendations for permanent prostate brachytherapy postimplant dosimetric analysis. *International Journal of Radiation Oncology* Biology* Physics*, 46(1):221–230, 2000.

[16] Tyler Harrison and Roger J Zemp. Coregistered photoacoustic-ultrasound imaging applied to brachytherapy. *Journal of Biomedical Optics*, 16(8):080502–080502, 2011.

[17] Jimmy L Su, Richard R Bouchard, Andrei B Karpiouk, John D Hazle, and Stanislav Y Emelianov. Photoacoustic imaging of prostate brachytherapy seeds. *Biomedical optics express*, 2(8):2243, 2011.

[18] E. M. Boctor. Prostate brachytherapy seed localization using combined photoacoustic and ultrasound imaging. In *Medical Imaging 2010, Ultrasonic Imaging, Tomography and Therapy, San Diego, California, Poster Session Paper No. 7629-29, SPIE*, 14 February 2010.

[19] Minghua Xu and Lihong V Wang. Photoacoustic imaging in biomedicine. *Review of scientific instruments*, 77(4):041101–041101, 2006.

[20] Nathanael Kuo, Hyun Jae Kang, Danny Y Song, Jin U Kang, and Emad M Boctor. Real-time photoacoustic imaging of prostate brachytherapy seeds using a clinical ultrasound system. *Journal of biomedical optics*, 17(6):0660051–0660057, 2012.

[21] Leo Pan, Ali Baghani, Robert Rohling, Purang Abolmaesumi, Septimiu Salcudean, and Shuo Tang. Improving photoacoustic imaging contrast of brachytherapy seeds. In *SPIE BiOS*, pages 85814B–85814B. International Society for Optics and Photonics, 2013.

[22] Muyinatu A Lediju Bell, Nathanael Kuo, Danny Y Song, and Emad M Boctor. Short-lag spatial coherence beamforming of photoacoustic images for enhanced visualization of prostate brachytherapy seeds. *Biomedical Optics Express*, 4(10):1964, 2013.

[23] Behnaz Pourebrahimi, Sangpil Yoon, Dustin Dopsa, and Michael C Kolios. Improving the quality of photoacoustic images using the short-lag spatial coherence imaging technique. In *SPIE BiOS*, pages 85813Y–85813Y. International Society for Optics and Photonics, 2013.

[24] M. A. Lediju, G. E. Trahey, B. C. Byram, and J. J. Dahl. Short-lag spatial coherence of backscattered echoes: Imaging characteristics. *IEEE Transactions on Ultrasonics, Ferroelectrics and Frequency Control*, 58(7):1337, 2011.

[25] R. J. Fedewa, K. D. Wallace, M. R. Holland, J. R. Jago, G. C. Ng, M. R. Rielly, B. S. Robinson, and J. G. Miller. Spatial coherence of the nonlinearly generated second harmonic portion of backscatter for a clinical imaging system. *IEEE Transactions on Ultrasonics, Ferroelectrics and Frequency Control*, 50(8):1010–1022, 2003.

[26] ANSI Standard. Z136. 1. American national standard for the safe use of lasers. American National Standards Institute. *Inc., New York*, 1993.